

A Random Forest Regression Based Space Vector PWM Inverter Controller for the Induction Motor Drive

M. A. Hannan, *Member, IEEE*, Jamal Abd Ali, Azah Mohamed, *Senior Member, IEEE*, and Mohammad Nasir Uddin, *Senior Member, IEEE*

Abstract—This paper presents a random forest (RF) regression based implementation of space vector pulse width modulation (SVPWM) for a two-level inverter to improve the performance of the three-phase induction motor (TIM) drive. The RF scheme offers the advantage of rapid implementation and improved prediction for the SVPWM algorithm to improve the performance of a conventional space vector modulation scheme. In order to show the superiority of the proposed RF technique to other techniques, an adaptive neuro fuzzy inference system (ANFIS) and artificial neural network (ANN) based SVPWM schemes are also used and compared. The proposed speed controller uses a backtracking search algorithm to search for the best values for the proportional-integral controller parameters. The robustness of the RF-based SVPWM is found superior to the ANFIS and ANN controllers in all tested cases in terms of damping capability, settling time, steady-state error, and transient response under different operating conditions. The prototype of the optimal RF-based SVPWM inverter controller of induction motor drive is fabricated and tested. Several experimental results show that there is a good agreement of the speed response and stator current with the simulation results which are verified and validated the performance of the proposed RF-based SVPWM inverter controller.

Index Terms—Adaptive neuro fuzzy inference system (ANFIS), artificial neural network (ANN), backtracking search algorithm (BSA), induction motor (IM), inverter controller, random forest (RF) regression, space vector pulse width modulation (SVPWM).

I. INTRODUCTION

OVER the last several decades voltage source inverter (VSI) based variable frequency drive has been widely utilized

Manuscript received December 1, 2015; revised May 10, 2016 and August 3, 2016; accepted October 19, 2016. Date of publication November 21, 2016; date of current version March 8, 2017.

M. A. Hannan is with the Department of Electrical Power Engineering, College of Engineering, Universiti Tenaga Nasional, Kajang 43000, Malaysia (e-mail: hannan@uniten.edu.my).

J. A. Ali and A. Mohamed are with the Department of Electrical, Electronic and System Engineering, Universiti Kebangsaan Malaysia, Bangi 43600, Malaysia (e-mail: eng_jhy@yahoo.com; azah_mohamed@ukm.edu.my).

M. N. Uddin is with the Department of Electrical Engineering, Lakehead University, Thunder Bay, ON P7B 5E1, Canada (e-mail: mud-din@lakeheadu.ca).

Color versions of one or more of the figures in this paper are available online at <http://ieeexplore.ieee.org>.

Digital Object Identifier 10.1109/TIE.2016.2631121

in various industrial applications, such as power supplies, active filter, and induction motor (IM) drives [1]–[3]. The performance of VSI depends on the switching control scheme of the insulated-gate bipolar transistors (IGBTs) in the inverter for generating less harmonic waveforms [2]. There are many switching control techniques, such as sinusoidal pulse width modulation (SPWM), space vector pulse width modulation (SVPWM), carrier-based PWM, selective harmonic elimination PWM, and harmonic band PWM, respectively, [3]. Among previous control schemes the SVPWM technique is the best method for VSI because of lower switching losses and its ability to minimize the harmonic output signals produced by the inverter [2], [4]–[10]. In [8], Piao and Hung reported a unified SVPWM technique for a multilevel inverter that requires complex nonlinear calculation involving modulation implicit functions of SVPWM. In general, most of the SVPWM requires complex online computation which leads to difficulty in real-time implementation. That is why only simulation results are presented in [8]. Thus, the conventional SVPWM requires additional memory that limits the choices of switching frequency and thereby reducing the accuracy of SVPWM [2], [7], [10]. To solve this problem genetic algorithm (GA) based SVPWM is utilized [11], but the GAs require much iteration to find the best results, which is time consuming. An artificial neural network (ANN) is also used in SVPWM [7], [10] for efficient inverter operation. In [2], the adaptive neural fuzzy inference system (ANFIS) based SVPWM is used for the two-level inverters. However, the above-mentioned methods encountered problems because of their huge data requirement, long training, and learning times of linear and nonlinear functions that consume huge memory for real-time implementation.

Many contemporary research work used new machine learning techniques to overcome the problems of artificial intelligence. One of the most important of these methods is the random forests (RF) regression technique, which has been used to develop the actual image spectra [12], and to improve rainfall rate assignment during day, night, and twilight [13]. In [14], Lindner *et al.* used RF regression to vote for the optimal positions, leading to robust and accurate results. RF regression is also used to choose groups of the metabolites and transcripts which show association with potato tuber flesh color and enzymatic discoloration [15]. In [16], RF techniques are used to improve image segmentation and to predict churn in the banking

industry, respectively. Therefore, this paper proposes the RF regression based SVPWM technique to minimize the complex online computation required for real-time implementation. This is a cost-effective approach that does not limit the choices of switching frequencies for linear and nonlinear functions and, thus, it leads to fast and accurate results. RF gives the results through predictors in each tree depending on the probability and the statistical operations. It produces better results than those of both ANFIS and ANN techniques.

Over the years, proportional-integral-derivative (PID) controllers have been widely used for a three-phase induction motor (TIM) in industrial applications due to its easy implementation, simple design, and structure [17], [18]. However, it requires a mathematical model and a trial and error procedure to find the best PID control parameters [17]–[19]. This paper uses backtracking search algorithm (BSA) to overcome these problems through a search for the best values of the PI speed controller parameters. In this paper, a prototype of the RF-based SVPWM inverter controller is implemented to justify the simulation results by the experimental results and to validate the performance of the proposed controller.

II. SVPWM SWITCHING TECHNIQUE

The SVPWM technique used the inverter states to generate firing pulses for the inverter switches [11], [20]. The SVPWM has been improved to achieve higher output voltage, minimum harmonic output, and reduction of the switching losses when compared with other PWM techniques [6]. Thus, the conventional SVPWM, ANN-based SVPWM, and ANFIS-based SVPWM schemes are discussed below.

A. Conventional SVPWM for a Two-Level Inverter

The VSI of the two-level type has a dc source and six switching devices including three upper and three lower switches, respectively. IGBTs are the most common switches for the inverter because of their fast switching, easy control, and high efficiency capabilities [19], [22]. The optimized three-phase voltages are generated by the V/f control for IM drive with conventional SVPWM. The three-phase voltage (V_a, V_b, V_c) can be converted to two-phase voltage (V_α, V_β) using Clark's transformation as [6]

$$\begin{bmatrix} V_\alpha \\ V_\beta \end{bmatrix} = \frac{2}{3} \begin{bmatrix} 1 & -1/2 & -1/2 \\ 0 & \sqrt{3}/2 & -\sqrt{3}/2 \end{bmatrix} \begin{bmatrix} V_a \\ V_b \\ V_c \end{bmatrix}. \quad (1)$$

The two-phase voltages V_α and V_β are used to compute the magnitude of reference voltage vector and angular between voltages as [19], [22]

$$|V_{ref}| = \sqrt{V_\alpha^2 + V_\beta^2} \quad (2)$$

$$\alpha = \tan^{-1} \left(\frac{V_\beta}{V_\alpha} \right). \quad (3)$$

Each output signal cycle is divided into six sectors in the shape of a hexagon [6]. The reference voltage (V_{ref}) and theta (α) in each sector are the products of two adjacent nonzero vectors and zero vectors, respectively. The hexagon consists of the six

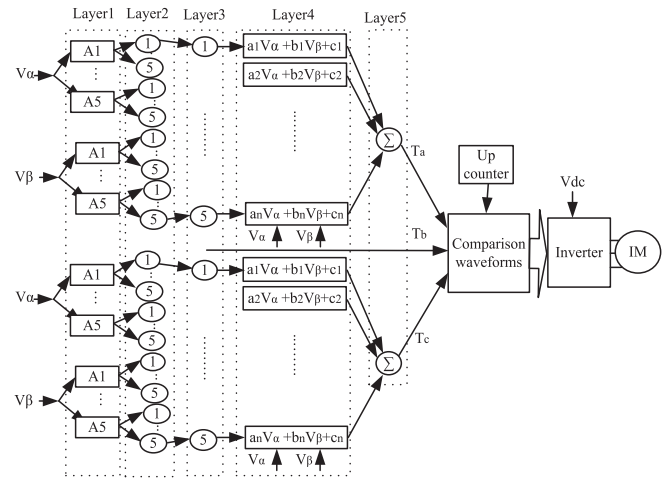


Fig. 1. Structure ANFIS-based SVPWM for a two-level inverter.

nonzero vectors (i.e., V_1, V_2, \dots, V_6) and two zero vectors (i.e., V_0, V_7). V_{ref} and α inside the hexagon can be calculated time shared T_1, T_2 through its two adjacent vectors as shown in the following equations [6], [11], [18]:

$$T_1 = \frac{\sqrt{3} \cdot T_s \cdot |V_{ref}|}{V_{dc}} \sin \left(\frac{n}{3} \pi - \alpha \right) \quad (4)$$

$$T_2 = \frac{\sqrt{3} \cdot T_s \cdot |V_{ref}|}{V_{dc}} \sin \left(\alpha - \frac{n-1}{3} \pi \right) \quad (5)$$

$$T_0 = T_s - (T_1 + T_2) \quad (6)$$

where $n = 1 - 6$ sectors at $0 \leq \alpha \leq \pi/3$; T_1, T_2 , and T_0 are the time vectors of the respective voltage vectors; T_s is the switching time; and α is the angle of the reference vector relative to space vector. The PWM control has an important factor known as the modulation index (MI), which is an important part for improving the accuracy through decreasing total harmonic distortion of the inverter output signals. The MI is defined as follows [19], [23]:

$$MI = \frac{V_{p1}}{V_{p1six}} \quad (7)$$

where V_{p1} is the maximum value of the fundamental voltage and V_{p1six} is the maximum value of the fundamental voltage at a six-step operation. Accordingly, $V_{p1six} = \frac{2}{\pi} V_{dc}$, where V_{dc} is the dc-link voltage [2]. The SVM technique only computes the time shares of the space vectors and does not specify the location in which they are applied [21], [22].

B. ANFIS-Based SVPWM

The fuzzy system and a neural network have their own merits and demerits. This has led to increased interest in mixing between fuzzy and neural network to take advantage from them. The result has generated a new method called ANFIS. ANFIS consists of a many layered and feedforward network [24], [25]. Fig. 1 shows the developed ANFIS-based SVPWM (ANFIS-SVM) for a two-level inverter based TIM drive. V_α and V_β voltages are fed to the ANFIS to create the duty ratios (T_a, T_b, T_c).

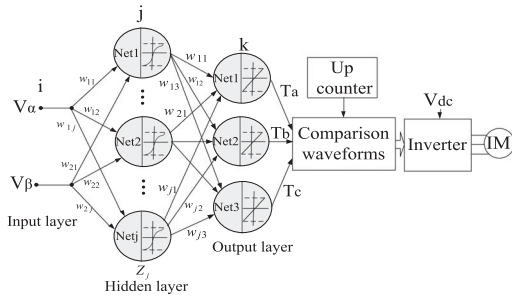


Fig. 2. Structure ANN-based SVPWM for a two-level inverter.

These duty ratios are compared with the waveforms during the switching time (T_s) to create the switching pulses for the inverter. Thus, it requires three structures of the ANFIS to give three outputs. Each structure has two inputs and one output, as shown in Fig. 1.

The first-order Takagi–Sugeno fuzzy model is used as a typical rule set with two inputs V_α and V_β with a function response f_1, f_2, \dots, f_n which can be given in generalized form as [24]:

Rule 1: If V_α is A_1 and V_β is B_1 , then $f_1 = a_1 V_\alpha + b_1 V_\beta + c_1$

Rule 2: If V_α is A_2 and V_β is B_2 , then $f_2 = a_2 V_\alpha + b_2 V_\beta + c_2$

⋮

Rule n : If V_α is A_i and V_β is B_i , then $f_n = a_n V_\alpha + b_n V_\beta + c_n$

where $n = 1, 2, \dots$ and $i = 1, 2, \dots$, respectively, A_i, B_i are membership functions (MFs) for inputs V_α, V_β , and a_n, b_n, c_n are parameters of the Takagi–Sugeno model. The ANFIS architecture consists of five layers, namely, the fuzzy layer, product layer, normalized layer, defuzzification layer, total output layer with rules and MFs connected with each input.

The ANFIS inputs are V_α and V_β that interference for each node from A_i and B_i . A_i and B_i are the linguistic functions used in the fuzzy theory to define MFs and uses five MFs and triangular functions type. The triangle MFs are represented in the following equation [25]:

$$F(x; z, c, m) = \begin{cases} \frac{x-z}{c-z} & z \leq x < c \\ \frac{x-m}{c-m} & c \leq x < m \end{cases} \quad (8)$$

where the parameters z and m are bound to the width of the triangular function and the parameter c located at the centre of the triangular function. The details about each layer of the ANFIS are given below [24], [25].

C. ANN-Based SVPWM

ANN is used as a solution to problems, such as power system stability estimation, IM control, and power electronic systems due to its rapid implementation [2]. Fig. 2 shows the block diagram of the ANN-based SVPWM (ANN-SVM) for a two-level inverter based IM drive. Two voltages (V_α and V_β) are fed to the ANN to create the duty ratios (T_a, T_b, T_c). These

duty ratios are compared with the waveforms in the switching time (T_s) to create the switching pulses for the inverter. Among many types of ANN the back-propagation (BP) neural network (NN) (shown in Fig. 2) is used due to its multilayered, fully connected, and feedforward structure.

The BP-NN structure consists of three layers. The number of nodes in the input, hidden, and the output layers are 2–40–3 nodes, respectively. The input layer consists of two inputs V_α and V_β , hidden layers of N -nodes, and the output layer of three outputs (T_a, T_b, T_c). The tangent-sigmoid activation functions reside in the hidden layer and linear activation functions are assigned to the output layer neurons. Equations (9) and (10) show the hidden layer and output layer responses, respectively,

$$\text{net}_j = \sum_{i=1}^P w_{ij} x_i + b_{oj}, \quad Z_j = f(\text{net}_j) \quad (9)$$

$$\text{net}_K = \sum_{j=1}^M w_{jk} Z_j + b_{ok}, \quad Y_K = f(\text{net}_K) \quad (10)$$

where $x_i, i = 1, 2$, is inputs value, $Z_j, j = 1, 2, \dots, 40$, is outputs hidden layer, and $Y_k, k = 1, 2, 3$, is outputs value. The ANN can be trained through the batch mode that is used here and the training data used for training ANN are taken from C-SVPWM through operating the system and saving.

III. RANDOM FOREST REGRESSION

The RF method, which was first proposed by Breiman in 2001, is a set of predictors that depend on trees in the forests through the random input values of each tree [27]. The RF regression consists of many trees and selects random subsets of the number of different predictors tested at each node. To build or grow the trees, a deterministic algorithm is developed to select each tree from a random set of variables and the training data are taken as random sample [12]. The node is used to divide the nodes for minimizing from the total number through description available for analysis. The sampled random vector and standard RF are mixed as predictors for each tree with the same distribution for all trees in the forest [12], [26].

A. RF Regression Algorithm

The RF regression consists of the input vector $X = \{x_1, x_2, \dots, x_p\}$, where a p -dimensional input vector that works in building a forest. Inside the forest a set of K trees $\{T_1(x), T_2(x), \dots, T_k(x)\}$, the output of each tree predicts the outputs for actual value $\{\hat{Y}_1 = T_1(X), \dots, \hat{Y}_m = T_m(X)\}$, where $m = 1, \dots, K$. The final result of the RF calculated through an average of all trees predictions by the following equation [27]:

$$\text{Predict}_{\text{RF}}(X) = \frac{1}{k} \sum_{k=1}^K \hat{Y}_k(X). \quad (11)$$

The training dataset is assumed to be independently drawn from the input and output $D = \{D_1, D_2, \dots, D_n\} = \{(x_1, y_1), (x_2, y_2), \dots, (x_n, y_n)\}$, where $x_i, i = 1, \dots, n$, is the training dataset for the input vector and $y_i, i = 1, \dots, n$, is the training dataset for the output vector. Each tree is grown

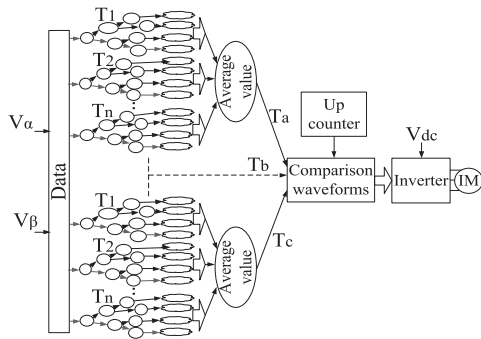


Fig. 3. Structure of the RF regression based SVPWM for a two-level inverter.

through the training procedure mentioned in [13]. The estimated error and accuracy is evaluated for the RF regression through the minimization of the mean square error (MSE). Finding the optimum trees in the forest depends on the MSE as shown in (12). Testing data passed through each split node, by sending it either to the right or to the left child until ending up at a leaf node [25].

$$\text{MSE} \approx \text{MSE}^{\text{OOB}} = \frac{1}{n} \sum_{i=1}^n \left(\hat{Y}(X_i) - Y_i \right)^2 \quad (12)$$

where $\hat{Y}(X_i)$ is the predicted output of the trees in the forest corresponding to a given input sample, Y_i is the observed output, and n represents the total number of out-of-bag (OOB) samples.

B. RF Regression Based SVPWM

Fig. 3 represents the proposed RF regression based SVPWM (RF-SVM) on the two-level inverter for the IM. V_α and V_β voltages are fed to the RF regression model to create the duty ratios (T_a, T_b, T_c). These duty ratios are compared with the waveforms in the switching time (T_s) to create the switching pulses for the inverter switches. In this paper, three structures of the RF regression are required due to three outputs. Each structure has two inputs and one output, as shown in Fig. 3. The RF regression has many trees fully built by using the available training data. After training, regression trees can be used for prediction corresponding to unknown data. However, the RF algorithm has the difficulties in selecting the best number of trees to design the system. In this paper, the training of RF-SVM is adjusted to select the number of trees. Five RF models including number of trees of 25, 50, 75, 100, and 125, respectively, are created to select the optimal number of trees. It is observed that the MSE of the 100 trees is approximately similar to that of 125 trees. Therefore, in an RF model, 100 trees are regarded as the sufficient trees to reduce the complexity in computation and achieve fast response. The detail algorithm for the proposed RF regression based SVPWM training is given in Table I.

IV. OVERALL CONTROL SYSTEM

The block diagram of the closed-loop V/f (V/Hz) controlled SVPWM inverter based TIM drive is shown in Fig. 4. For comparison purpose the inverter control includes proposed and

TABLE I
RF REGRESSION BASED SVPWM TRAINING ALGORITHM

Proposed RF regression based SVPWM training algorithm
1. Identify the inputs (V_α, V_β) and the outputs (T_a, T_b, T_c) for representing random forest regression model to the SVPWM.
2. Select the optimal number of trees (100 trees) to be grown in forests.
3. Grow each tree using bootstrap samples taken from the main dataset.
4. Calculate the prediction error to the regression trees which built using OOB and MSE as shown in (12).
5. During the application the system obtain trees output for an input which came from V/f control and observe the output RF regression and obtain the final output.

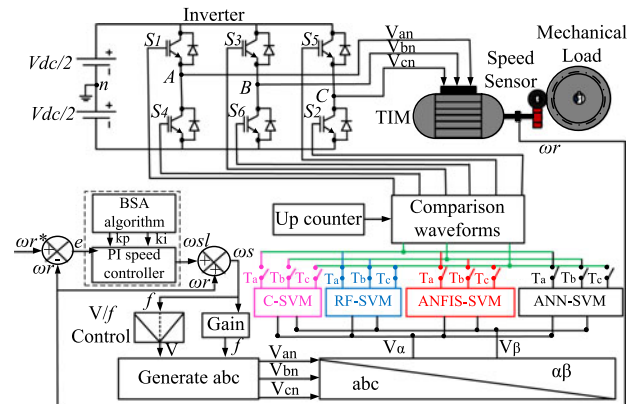


Fig. 4. Block diagram of the proposed RF regression for an SVPWM inverter.

conventional RF regression, ANFIS, and ANN-based SVPWM techniques. The task for each of these controllers is to force the TIM to follow the command speed. A PI speed controller is used to create the slip speed of the TIM. Corresponding to the rated flux linkage V/f control generates the peak voltage. The peak voltage and frequency generates the voltages V_α and V_β . These voltages are the inputs to the SVPWM to generate the switching pulses for the inverter.

C. Speed Controller Optimization Using BSA

The accurate parameters of the PI speed controller are difficult to find. Therefore, in the study first the parameters of the PI control are tuned by the BSA algorithm and then that optimized parameters are used for the proposed PI speed controller. The PI speed controller has nonseparable characteristic (k_p and k_i values are dependent on each other) and multimodal characteristic (good performance with different values). In this study, the BSA optimization technique is chosen due to its searching capabilities on finding the optimal PI parameters to support the nonseparable and multimodal characteristics. The principle of BSA for producing a trial population includes two new crossovers and mutation operators. BSA dominates the value of the search on the best populations and searches in the spaces boundary to find the very sturdy exploration and exploitation capabilities [19]. The BSA has been implemented to improve the PI speed controller. BSA design including initialization, selection-I, mutation, crossover, and selection-II is explained below.

Initialization process is the primitive configuration of population for the numerical values of PI control parameters (X_{ij}) demonstrated by the following equation:

$$X_{ij} = \text{rand.} \cdot (\text{up}_j - \text{low}_j) + \text{low}_j \quad (13)$$

where $i = 1, 2, \dots, N$, N is population size, and $j = 1, 2, \dots, P$, P is the problem dimension.

The historical population ($\text{old}X_{ij}$) to be used for calculating the search direction is constructed by using the following equation:

$$\text{old}X_{ij} = \text{rand.} \cdot (\text{up}_j - \text{low}_j) + \text{low}_j. \quad (14)$$

The $\text{old}X_{ij}$ remembers the population from a randomly chosen previous generation for creating the search-direction matrix, taking partial advantage of previous experiences to generate a new trial population. The comparison between two random values is shown in the following condition:

$$\text{if } a < b, \quad \text{then } \text{old}X_{ij} := X_{ij} \quad (15)$$

$$\text{old}X_{ij} = \text{permuting}(\text{old}X_{ij}). \quad (16)$$

Mutation is a process that produces a new population of the initial and history population, as shown in (17), in which F value controls the amplitude of the search-direction matrix

$$\text{Mutant} = X_{ij} + F \cdot \text{randn.}(\text{old}X_{ij} - X_{ij}). \quad (17)$$

BSA generates a trial population, and then takes a partial advantage of its experiences from previous generations. In this process, the trial population H_{ij} is generated. The initial of the trial populations is taken from mutation, as shown in (17). The crossover consists of two parts. The first part generates the binary matrix called map_{ij} , and the second part is the process comparison between population X_{ij} and trial population H_{ij} . Crossover is used to obtain updates map_{ij} . In addition, this part works on control mechanism of boundaries for the trial population. An optimization process runs to compare the population X_{ij} and trial population H_{ij} to obtain the best population as well as objective value. The objective function for the BSA algorithm is the mean absolute error (MAE) of the speed which is designed to minimize the steady-state error, overshoot (OS)/undershoot, and settling time (ST). The detail functional flow of the BSA-based PI speed controller is shown in Fig. 5(a) and Fig. 5(b) explains the relationship between iteration and objective function.

V. EXPERIMENTAL SETUP

In this paper, TIM is used a WEG standard 4-poles of 1.0 HP, 50 Hz, and 415 V. The parameters of the TIM are shown in Table II. A three-phase inverter is used to drive the TIM with the switching frequency of 20 kHz and a dead time $5 \mu\text{s}$. The BSA-PI speed controller is implemented using a DSP-TM320F28335 controller and received the actual rotor position by enhance-quadrature encoder pulse (eQEP). The task of this controller is to allow the real speed to track the reference speed.

The experimental setup includes a DSP board that is connected to a personal computer by USB cable. The BSA-PI

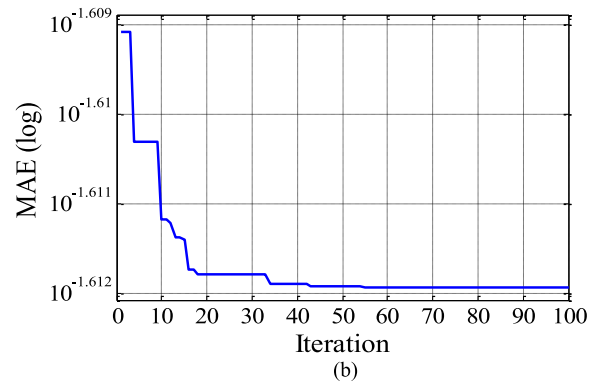
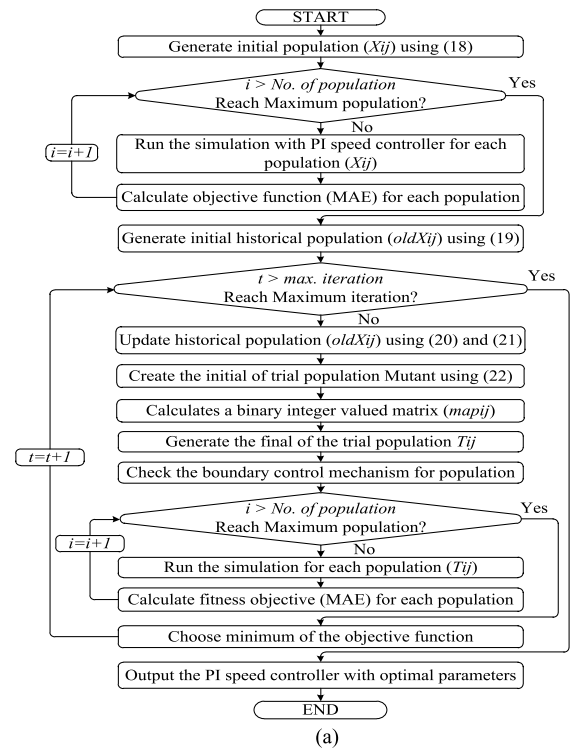


Fig. 5. (a) Flowchart for a BSA-PI controller and (b) objective function curve.

TABLE II
PARAMETERS OF THE IM

Definition	Values
Nominal power	1 HP
Nominal voltage	415 V
Nominal speed	1405 r/min
Stator resistance	13.6261 Ω
Rotor resistance	5.58466 Ω
Stator leakage inductance	23.2348 mH
Rotor leakage inductance	28.7288 mH
Stator leakage reactance	7.29945 Ω
Rotor leakage reactance	9.02542 Ω
Mutual reactance	190.158 Ω
Nominal frequency	50 Hz
Number of poles	4
Moment of inertia	0.00225 $\text{kg} \cdot \text{m}^2$

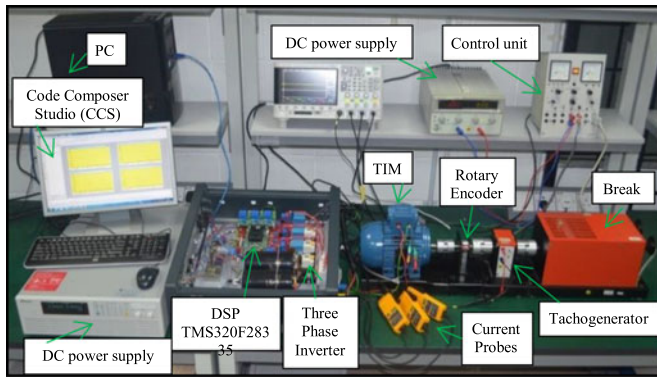


Fig. 6. Experimental setup of an RF-based SVPWM inverter controller for TIM.

speed controller program in MATLAB/Simulink is automatically generated C-code file using code composer studio (CCS) development environment. This program code is built-in in the DSP control board by USB cable from PC. The real rotor speed of the TIM is measured by a rotary encoder (E40H12-2000-3-T-24) of 2000 pulses per revolution and connected with DSP through eQEP. The DSP generate six SVPWM signals through gate pulse generator and pass the switching signal to the IGBTs gate of the inverter. The inverted voltage is then supplied to the TIM, as shown in Fig. 6.

The mechanical load of TIM is represented the magnetic power brake connected with its control unit. DC power supply is used to supply specific voltage to the magnetic power brake control unit and measured $1 \text{ V} = 1 \text{ N} \cdot \text{m}$. However, for measuring speed response, tacho-generator is linked to the rotor shaft of the motor. The tacho-generator constant is determined as 0.111 mV based on ration of tacho-generator output and speed response which is equal to 1 r/min . Also, for measuring stator, oscilloscope current probe (FLUKE) is utilized with ratio of 100 mV/A in each phase.

VI. RESULTS AND DISCUSSION

The performance of the RF regression based SVPWM (RF-SVM) is investigated in simulation using MATLAB/Simulink and compared with the conventional SVM (C-SVM), ANFIS, and ANN-based SVM to show the superiority of the proposed technique. Several experimental results are analyzed and compared with simulation results to justify the optimal performance of the RF-SVM based inverter controller. Statistical analysis for one cycle of duty ratio (T_a) is also analyzed between the techniques. Details of simulation and experimental results are explained under different case studies as follows.

A. Case-1: Step Changes in Reference Speed at No Load Condition

The performance of various SVM-based TIM drives for step changes in reference speed is shown in Fig. 7. The speed responses, stator currents, corresponding “a” duty ratios (T_a) and the duty ratio errors are shown in Fig. 7(a)–(d) at no load

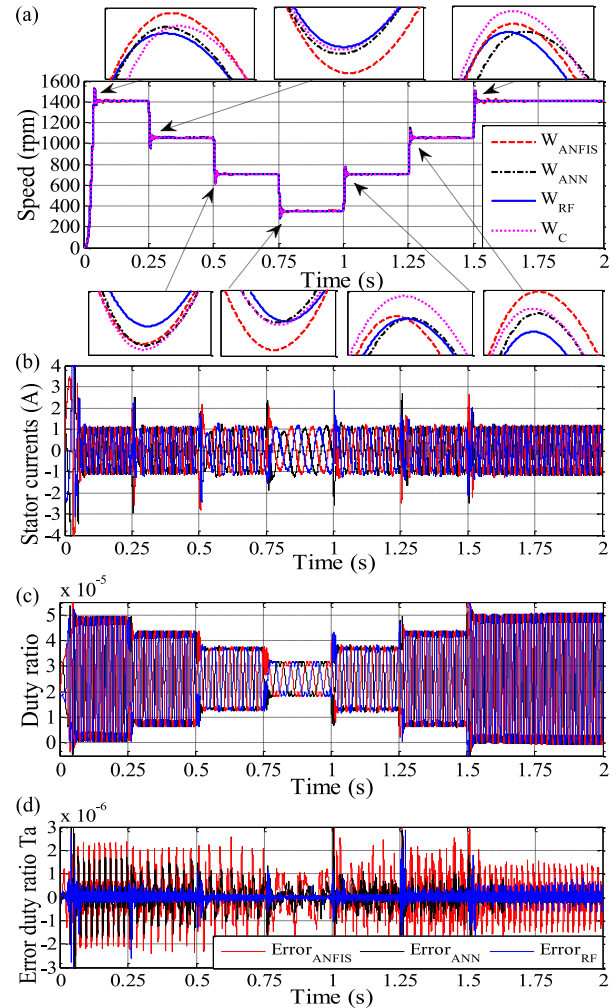


Fig. 7. (a) Speed response with sudden change in reference speed, (b) stator currents, (c) full duty ratio for RF-SVM, and (d) duty ratio error for T_a .

TABLE III
PERFORMANCE COMPARISON OF VARIOUS SVM TECHNIQUES FOR CASE-1

Speed (r/min)	1405	1054	702	351	702	1054	1405	
Time (s)	0	0.25	0.5	0.75	1	1.25	1.5	
C-SVM	OS	8.63	8.72	12.24	16.73	11.29	8.25	7.82
	ST	0.640	0.036	0.029	0.027	0.028	0.027	0.030
RF-SVM	OS	8.29	8.64	10.20	16.48	10.34	7.25	6.93
	ST	0.640	0.030	0.025	0.026	0.024	0.022	0.030
ANN-SVM	OS	8.53	9.00	11.70	16.62	10.47	8.97	6.93
	ST	0.680	0.051	0.025	0.041	0.031	0.028	0.150
ANFIS-SVM	OS	9.18	9.63	11.97	18.66	10.40	8.15	7.34
	ST	0.650	0.100	0.032	0.029	0.120	0.110	0.030

condition, respectively. Performance comparisons among various SVM techniques are summarized in Table III. For comparison purpose, OS %, and ST for speed responses are considered as performance measuring parameters. It is found that the proposed RF-SVM technique has the least OS and ST among all the SVM techniques, as given in Table III and which can also

TABLE IV
PERCENTAGE IMPROVEMENT OF OS AND ST FOR CASE-1

Speed (r/min)		1405	1054	702	351	702	1054	1405
Time (s)		0	0.25	0.5	0.75	1	1.25	1.5
RF-C	OS %	3.9	0.9	16.6	1.4	8.4	12.1	11.3
	ST %	0	16.1	13.7	3.7	14.2	18.5	0
RF-ANN	OS %	2.8	4	12.8	0.8	1.2	19.1	0
	ST %	5.8	41.1	0	36.5	22.5	27.2	80
RF-ANFIS	OS %	9.6	10.2	14.7	11.6	0.5	11	5.5
	Acc.ST %	1.5	70	21.8	10.3	9.6	80	0

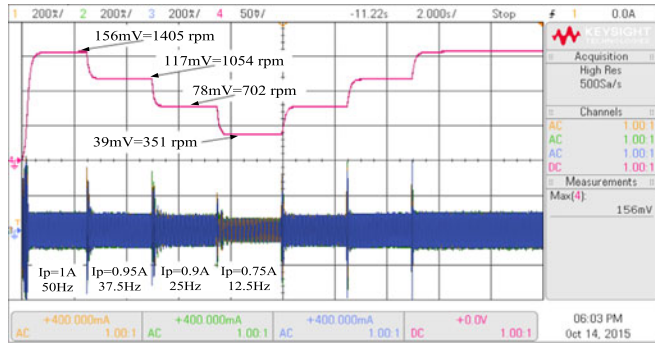


Fig. 8. Experimental result of step speed responses and stator currents.

be seen from zoom-in view of the speed response in Fig. 7(a). Fig. 7(b) shows the stator currents, the variable frequency, and constant peak values were changed by step changes in reference speed for a specific duration because the speed is directly proportional to frequency.

The duty ratio errors are calculated for RF-SVM, ANN-SVM, and ANFIS-SVM techniques compared with the duty ratio of the C-SVM technique. That means the error duty ratio of RF for T_a is $\text{Error}_{\text{RF}} = T_{a_{\text{conv}}} - T_{a_{\text{RF}}}$. Similarly, for ANN and ANFIS, the error duty ratios are $\text{Error}_{\text{ANN}} = T_{a_{\text{conv}}} - T_{a_{\text{ANN}}}$ and $\text{Error}_{\text{ANFIS}} = T_{a_{\text{conv}}} - T_{a_{\text{ANFIS}}}$, respectively, as shown in Fig. 7(c). The MAE of duty ratios is calculated at the time when the speed changes and the results are found as MAE-RF is $5.0636e-8$, and MAE-ANN and MAE-ANFIS are $3.2949e-7$ and $6.8106e-7$, respectively. Thus, it confirms that the proposed RF-SVM technique produced fewer errors than any other techniques. The percentage (%) improvement of the system performance between RF responses and other techniques are computed for OS ($\frac{\text{OS}_{\text{technique}} - \text{OS}_{\text{RF}}}{\text{OS}_{\text{technique}}} \times 100\%$) and ST ($\frac{\text{ST}_{\text{technique}} - \text{ST}_{\text{RF}}}{\text{ST}_{\text{technique}}} \times 100\%$) for case 1 and case 2, as shown in Tables IV and VI. It is observed that in all speeds and times, the improvement of RF-SVM indices are significantly well compare to other techniques.

The experimental result illustrated in Fig. 8 applies to the up-to-down step speed test implementation shows the effectiveness of the proposed controller at no load condition. The experimental measurements were taken in a KEYSIGHT DSO-X2024A oscilloscope in duration of 2 s/Div which has four channels; three channels are representing stator current for phase a, b,

and c with 200 mA/Div and the fourth channel representing the speed response with 50 mV/Div. The experimental result shows the step up-to-down speed response of the TIM drive changed at 2.5 s as a step response from 156 to 117 mV which are equal to 1405 r/min and 1054 r/min, respectively. Similarly, the speed response of TIM drive changed at 5 s from 117 to 78 mV, at 7.5 s from 78 to 39 mV, and return to step up to full speed voltage of 156 mV, which are equal to 1054–702 r/min, 702–351 r/min and then the return step by step to full speed of 1405 r/min at no load condition. It can be seen in Fig. 8, the experimental results manage to establish the highest matching with the speed responses of the simulation result in Fig. 7(a) to validate the optimal performance of the RF-SVM based inverter controller. It is also noticed that the stator currents are achieved variation in the frequency due to relationship with variation speed which is similar with the variation of simulation results.

B. Case-2: Variation of Speed Response With Mechanical Load

This test aims to determine the system performance and robustness with the proposed techniques at variation speed with 4 N·m loads. The speed response and its zoomed locations in Fig. 9(a) show that the estimated speed is stated 1405 r/min until 0.3 s convert to 1054 r/min then convert to 1405 r/min at 0.6 s with applied 4 N·m for four SVM techniques. Fig. 9(b) shows the stator currents are constant peak value and variable frequency. Fig. 9(c) shows the fewer distortions in the duty ratio signal of RF-SVM at sudden change speed with load. The error calculation is the subtraction operation between conventional duty ratio (T_a) and any one of duty ratio of the proposed techniques such as $\text{Error}_{\text{RF}} = T_{a_{\text{conv}}} - T_{a_{\text{RF}}}$, $\text{Error}_{\text{ANN}} = T_{a_{\text{conv}}} - T_{a_{\text{ANN}}}$, and $\text{Error}_{\text{ANFIS}} = T_{a_{\text{conv}}} - T_{a_{\text{ANFIS}}}$, respectively, as shown in Fig. 9(d), which confirms that RF-SVM reduced more errors than the other techniques. The MAE of duty ratios are calculated at the time when the speed changes and the results are found as RF is $5.5619e-8$, ANN and ANFIS are $1.6447e-6$ and $1.0872e-6$, respectively. The obtained MAE from RF-SVM is better than other techniques. The OS and ST obtained from the RF-SVM technique are also better than that of other techniques under different speed responses of case-2, as shown in Table VI.

Fig. 10 shows the experimental result of speed responses and stator currents to determine the system performance and robustness of the proposed techniques at 3/4th of full speed variation with 4 N·m loads condition. In this case, an oscilloscope was set in 1 s/Div and the stator currents with 200 mA/Div and the speed response with 50 mV/Div, respectively. It can be seen that the speed response of the TIM changed at 3 s as a step response from 156 to 117 mV which are equal to 1405 and 1054 r/min, respectively, and then return step by step to full speed of 1405 r/min at 4 N·m load condition. The stator currents also have been changed due to the loading of TIM at 4 N·m within the step response of 3 and 6 s, respectively. It is worthwhile to mention that the change of speed response and stator currents in both simulation and experimental results are matched together at full to 3/4th of full speed variation with 4 N·m loads condition.

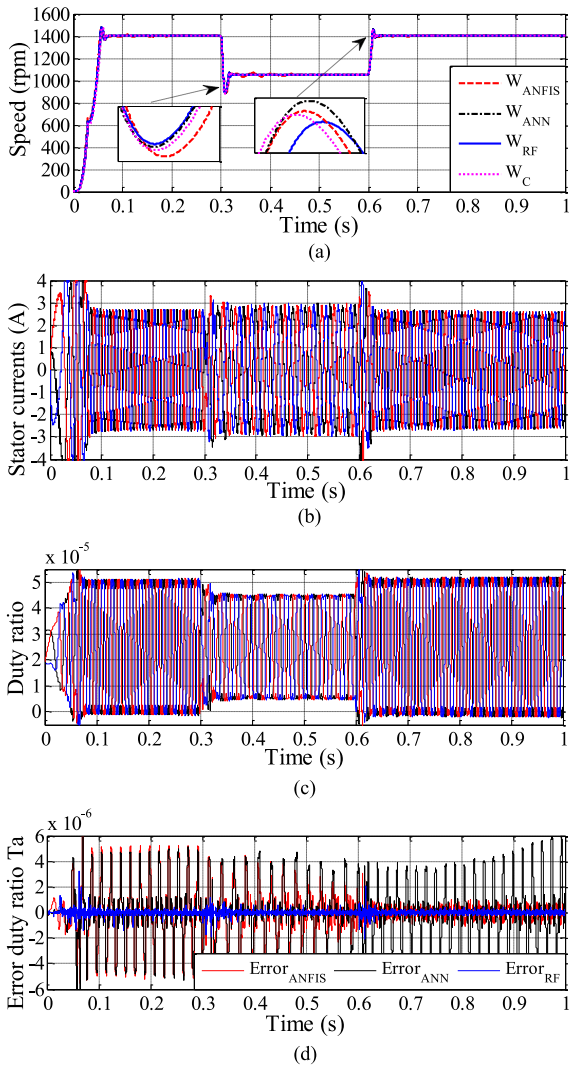


Fig. 9. (a) Variation speed response with 4 N·m load, (b) stator currents, (c) full duty ratio for RF-SVM, and (d) duty ratio error for T_a .

Fig. 11(a) shows that the estimated speed is fixed (i.e., 1405 r/min) for 0.3 s then it converts to 702 r/min until 0.6 s and again the speed step up to 1405 r/min until 1 s under applied load of 3.2 N·m. Fig. 11(b) shows that the peak stator currents are fixed with variable frequency. Fig. 11(c) shows the fewer distortions in the duty ratio signal of RF-SVM at sudden change speed with load. The error calculation is the subtraction operation between conventional duty ratio (T_a) and any one of duty ratio of the proposed techniques such as $ERROR_{RF} = T_{a_{conv.}} - T_{a_{RF}}$, $ERROR_{ANN} = T_{a_{conv.}} - T_{a_{ANN}}$, and $ERROR_{ANFIS} = T_{a_{conv.}} - T_{a_{ANFIS}}$, respectively, as shown in Fig. 11(d), which confirms that RF-SVM reduced more errors than the other techniques. The MAE of duty ratios is calculated at the time when the speed changes and the results are found as RF is $5.7598e-8$, and ANN and ANFIS are $1.0203e-6$ and $2.6496e-6$, respectively. The obtained results show that OS and ST are affected both with the change of speed at full to 3/4th and full to half speed with loads at 4 N·m and 3.2 N·m conditions, respectively, as shown in Table V. It is found that the RF-SVM has

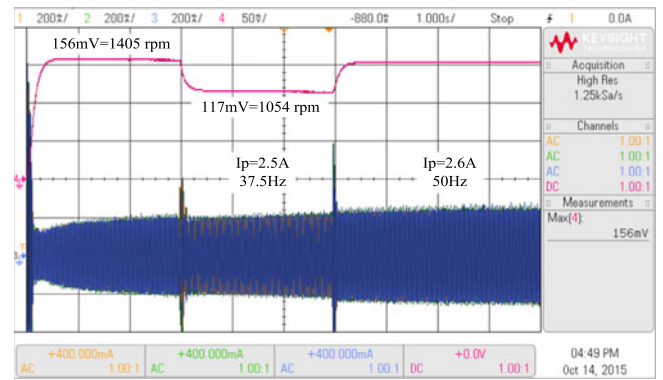


Fig. 10. Experimental results for speed response and stator currents at 4 N·m.

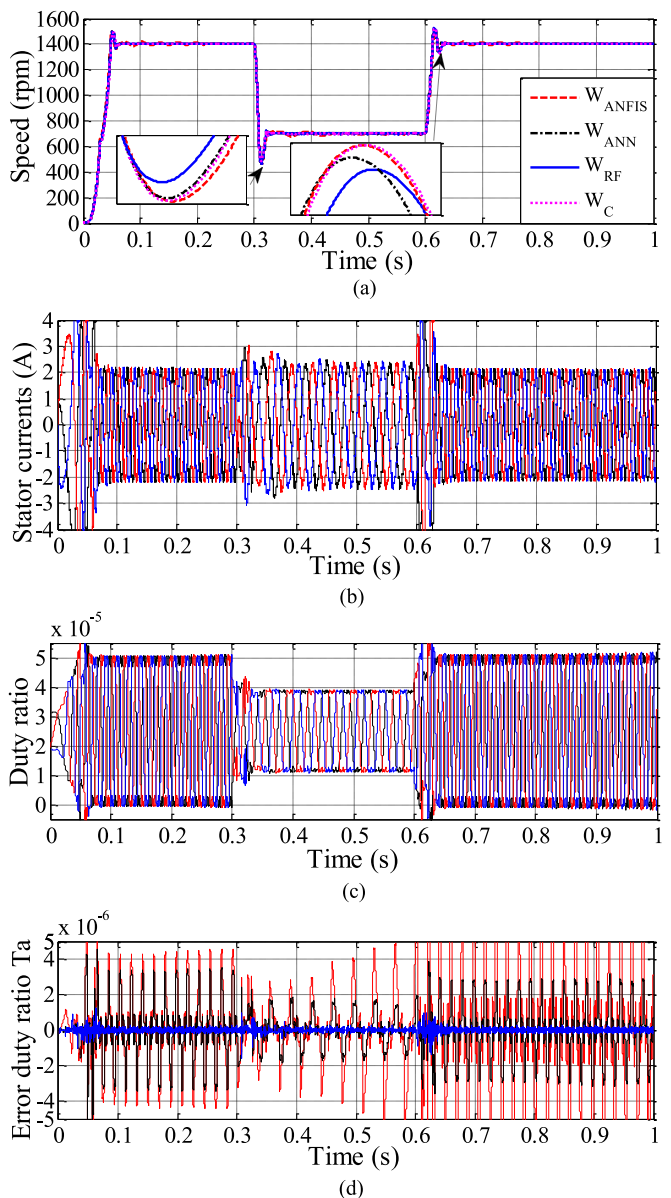


Fig. 11. (a) Variation speed response with 3.2 N·m load, (b) stator currents, (c) full duty ratio for RF-SVM, and (d) duty ratio error for T_a .

TABLE V
PERFORMANCE COMPARISON OF SVM TECHNIQUES FOR CASE-2

Speed (r/min)		1054	1405	702	1405
Time (s)		0.3	0.6	0.3	0.6
CSVM	OS	3.80	16.09	8.84	34.01
	ST	0.028	0.034	0.042	0.040
RF-SVM	OS	3.53	15.71	7.48	31.02
	ST	0.027	0.031	0.041	0.036
ANN-SVM	OS	4.21	15.95	8.09	33.34
	ST	0.030	0.037	0.045	0.039
ANFIS-SVM	OS	3.91	16.27	8.70	34.44
	ST	0.030	0.120	0.051	0.130

TABLE VI
PERCENTAGE IMPROVEMENT OF OS AND ST FOR CASE-2

Speed (r/min)		1054	1405	702	1405
Time (s)		0.3	0.6	0.3	0.6
RF-C	OS%	7.1	2.3	15.3	8.8
	ST%	3.5	8.8	2.3	10
RF-ANN	OS%	16.1	1.5	7.5	6.9
	ST%	10	16.2	8.8	7.6
RF-ANFIS	OS%	9.7	3.4	14	9.9

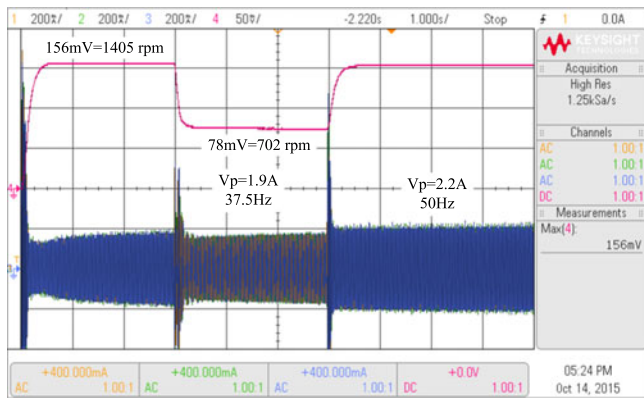


Fig. 12. Experimental results for speed response and stator currents at 3.2 N-m.

performed better than other techniques. Thus, it also confirms that the proposed RF-SVM produce least OS and ST than that of other techniques in case of variation speed response with of load (case-2). To show the superiority of RF-SVM, the percentage (%) improvement of the system performance is also calculated between RF responses and other techniques for case-2, as shown in **Table VI**.

Fig. 12 shows the experimental result of speed responses and stator currents at half speed variation with 3.2 N-m loads condition. It can be seen that the speed response of the TIM changed at 3 s as a step response from 156 to 78 mV, which are equal to 1405 and 702 r/min, respectively, and then the return step by step to full speed of 1405 r/min under 3.2 N-m load condition. The stator currents also have been changed due to the loading of TIM at 3.2 N-m within the step response of 3 and

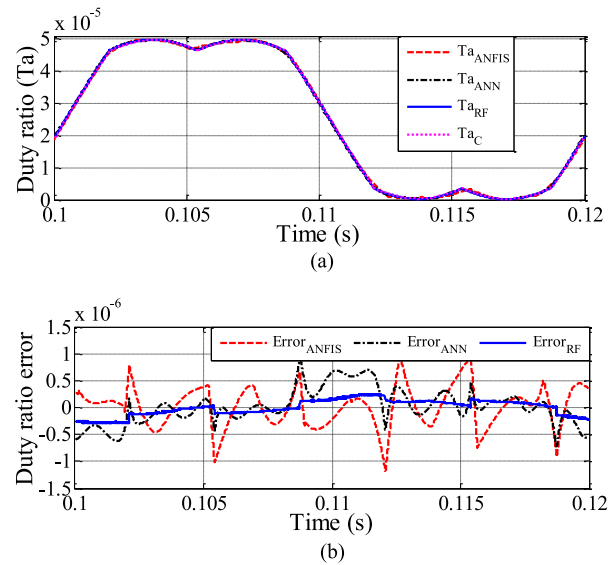


Fig. 13. (a) Duty ratio T_a for conventional and proposed techniques and (b) duty ratio error.

6 s, respectively. It is worthwhile to mention that the change of speed response and stator currents in both simulation and experimental results are matched together at full to half speed variation with 3.2 N-m load condition.

C. Case-3: Statistical Analysis

This study also demonstrated the statistical analysis utilizing the Bland-Altman method for one cycle of duty ratio (T_a) of C-SVM, RF-SVM, ANN-SVM, and ANFIS-SVM techniques, as shown in **Fig. 13(a)**. The error duty ratios are calculated between the C-SVM and the other techniques such as $ERROR_{RF} = T_{a_{conv.}} - T_{a_{RF}}$, $ERROR_{ANN} = T_{a_{conv.}} - T_{a_{ANN}}$, and $ERROR_{ANFIS} = T_{a_{conv.}} - T_{a_{ANFIS}}$, respectively, as shown in **Fig. 13(b)**. It is found that MAE produced $ERROR_{RF}$ is $1.2277e-7$, $ERROR_{ANN}$ is $2.4740e-7$, and $ERROR_{ANFIS}$ is $2.9486e-7$, respectively. Thus, it concludes that the RF-SVM is better in terms of producing less error than that of ANN-SVM and ANFIS-SVM techniques.

To show the symmetry or the difference between the proposed system and the conventional systems, the Bland-Altman duty ration plot is considered for RF-SVM, ANN-SVM, and ANFIS-SVM, respectively, as shown in **Fig. 14**. The Bland-Altman plot consists of three dotted lines such as the mean or average deference in the duty ratio, μ located at the center of the plot, upper limit of agreement, $\mu + 2\sigma$ and the lower limit of agreement, $\mu - 2\sigma$, respectively, where σ is a standard deviation for difference in duty ratio [28], [29]. **Fig. 14(a)** represents the difference between RF and conventional duty ratio, which shows that there is 99.75% of difference between limits of agreement ($2.89e-07$, $-2.89e-07$), the average or the mean difference is $2.3E-10$ and the standard deviation of the difference is $1.44E-07$. Similarly, **Fig. 14(b)** and **(c)** shows 95.997% and 94.01% differences in the duty ratio between their limits of agreements. It is found that a little duty ratio data lies out of regression lines as shown in

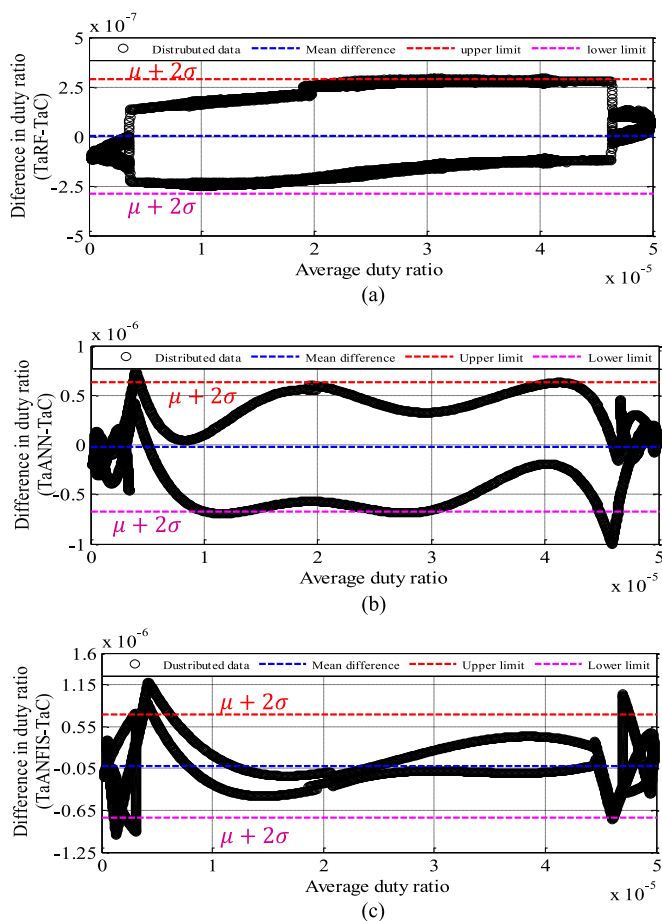


Fig. 14. Bland–Altman duty ratio plot between C-SVM and the (a) RF-SVM, (b) ANN-SVM, and (c) ANFIS-SVM.

the form of circles in Fig. 14. The observation indicates that the statistical analysis test results support and promote the operation of the proposed RF-SVM system relative to the conventional systems to show the better performance and effectiveness of the RF-SVM technique.

VII. CONCLUSION

This paper proposed a novel RF regression based SVPWM inverter controller for TIM drive to maximize damping capability and minimize ST, steady-state error, and transient response under different operating speed and load conditions. The idea of the proposed controller was to tune PI parameter by the BSA algorithm to find the best controller. An optimized speed controller then generates peak voltage by V/f control to SVPWM to generate the best switching pulse for the inverter. The objective function of the BSA algorithm was the MAE of the speed that was designed to minimize the steady-state error, OS/undershoot, and ST. The performance of the simulation model of the proposed RF-SVM technique is compared with the ANN- and ANFIS-based SVM techniques under different speed and load conditions. It was found that in each case, the performance of the RF-based SVPWM technique is superior to both ANN-SVM and ANFIS-SVM techniques in terms of damping capability, ST, steady-state error, and transient response under different operating speed and load conditions. This is due to the advantages

of RF regression which does not need large training data and requires less training time. Thus, the computation burden of the intelligent systems such as ANN- and ANFIS-based SVPWM techniques is removed. Hence, the RF-SVM technique can be implemented in real time using the DSP-TMS320F28335.

Accordingly, the prototype of the TIM drive was implemented with the proposed RF-based SVPWM inverter controller to show the effectiveness of the proposed technique under different speed and load conditions. It can be seen that the experimental results manage to establish the highest match with the speed responses and stator currents of the simulation results. Several experiments were conducted and found good agreement of the speed responses and stator currents with that of the simulation results, which verified and validated the performance of the optimal RF-SVM inverter controller as well as the success of the proposed technique.

REFERENCES

- [1] E. Levi, I. N. W. Satiawan, N. Bodo, and M. Jones, "A space-vector modulation scheme for multilevel open-end winding five-phase drives," *IEEE Trans. Energy Convers.*, vol. 27, no. 1, pp. 1–10, Mar. 2012.
- [2] D. G. Durgasukumar and M. K. Pathak, "Comparison of adaptive neuro-fuzzy-based space-vector modulation for two-level inverter," *Int. J. Elect. Power Energy Syst.*, vol. 38, no. 1, pp. 9–19, Jun. 2012.
- [3] C. Charumit and V. Kinnaree, "Discontinuous SVPWM techniques of three-leg VSI-fed balanced two-phase loads for reduced switching losses and current ripple," *IEEE Trans. Power Electron.*, vol. 30, no. 4, pp. 2191–2204, Apr. 2015.
- [4] P. Zheng, P. Wang, Y. Sui, C. Tong, F. Wu, and T. Li, "Near-five-vector SVPWM Algorithm for five-phase six-leg inverters under unbalanced load conditions," *J. Power Electron.*, vol. 14, no. 1, pp. 61–73, 2014.
- [5] Y. Fan, L. Zhang, M. Cheng, and K. Chau, "Sensorless SVPWM-FADTC of a new flux-modulated permanent-magnet wheel motor based on a wide-speed sliding mode observer," *IEEE Trans. Ind. Electron.*, vol. 62, no. 5, pp. 3143–3151, May 2015.
- [6] Z. Xueguang, Z. Wenjie, C. Jiameing, and X. Dianguo, "Deadbeat control strategy of circulating currents in parallel connection system of three-phase PWM converter," *IEEE Trans. Energy Convers.*, vol. 29, no. 2, pp. 406–417, Jun. 2014.
- [7] A. H. Bhat and P. Agarwal, "Implementation of a neural-network-based space vector pulse-width modulation for a three-phase neutral-point clamped high-power factor converter," *Elect. Power Compon. Syst.*, vol. 37, no. 2, pp. 210–233, Jan. 2009.
- [8] C. Piao and J. Y. Hung, "A simplified and unified space vector PWM algorithm for multilevel diode clamped VSI," in *Proc. IEEE Int. Conf. Ind. Technol.* 2015, pp. 2770–2776.
- [9] S. Pan, J. Pan, and Z. Tian, "A shifted SVPWM method to control dc-link resonant inverters and its FPGA realization," *IEEE Trans. Ind. Electron.*, vol. 59, no. 9, pp. 3383–3391, Sep. 2012.
- [10] N. Langer, A. H. Bhat, and P. Agarwal, "Neural-network-based space-vector pulse-width modulation for capacitor voltage balancing of three phase three-level improved power quality converter," *IET Power Electron.*, vol. 7, no. 4, pp. 973–983, Apr. 2014.
- [11] A. Mehrizi-Sani and S. Filizadeh, "An optimized space vector modulation sequence for improved harmonic performance," *IEEE Trans. Ind. Electron.*, vol. 56, no. 8, pp. 2894–2903, Aug. 2009.
- [12] O. Mutanga, E. Adam, C. Adjorlolo, and E. M. Abdel-Rahman, "Evaluating the robustness of models developed from field spectral data in predicting African grass foliar nitrogen concentration using worldview-2 image as an independent test dataset," *Int. J. Appl. Earth Obs. Geoinf.*, vol. 34, pp. 178–187, Feb. 2015.
- [13] M. Kühnlein, T. Appelhans, B. Thies, T. Nauss, and E. M. Abdel-Rahman, "Improving the accuracy of rainfall rates from optical satellite sensors with machine learning—A random forests-based approach applied to MSG SEVIRI," *Remote Sens. Environ.*, vol. 141, pp. 129–143, Feb. 2014.
- [14] C. Lindner, S. Thiagarajah, J. M. Wilkinson, G. A. Wallis, and T. F. Cootes, "Fully automatic segmentation of the proximal femur using random forest regression voting," *IEEE Trans. Med. Image.*, vol. 32, no. 8, pp. 1462–1472, Aug. 2013.

- [15] A. Acharjee *et al.*, "Data integration and network reconstruction with omics data using Random Forest regression in potato," *Anal. Chim. Acta*, vol. 705, no. 1/2, pp. 56–63, Oct. 2011.
- [16] D. Mahapatra, "Analyzing training information from random forests for improved image segmentation," *IEEE Trans. Image Process.*, vol. 23, no. 4, pp. 1504–1512, Apr. 2014.
- [17] J. Lee, M. Jin, and P. Chang, "Variable PID gain tuning method using backstepping control with time-delay estimation and nonlinear damping," *IEEE Trans. Ind. Electron.*, vol. 61, no. 12, pp. 6975–6985, Dec. 2014.
- [18] D. H. Lee and J. W. Ahn, "A simple and direct dead-time effect compensation scheme in PWM-VSI," *IEEE Trans. Ind. Appl.*, vol. 50, no. 5, pp. 3017–3025, Sep./Oct. 2014.
- [19] J. A. Ali, M. A. Hannan, A. Mohamed, and M. Abdolrasol, "Fuzzy logic speed controller optimization approach for induction motor drive using backtracking search algorithm," *Measurement*, vol. 78, pp. 49–62, Jan. 2016.
- [20] M. V. Rajkumar and P. S. Manoharan, "FPGA based multilevel cascaded inverters with SVPWM algorithm for photovoltaic system," *Sol. Energy*, vol. 87, pp. 229–245, Jan. 2013.
- [21] Z. Shu, N. Ding, J. Chen, H. Zhu, and X. He, "Multilevel SVPWM with dc-link capacitor voltage balancing control for diode-clamped multilevel converter based STATCOM," *IEEE Trans. Ind. Electron.*, vol. 60, no. 5, pp. 1884–1896, May 2013.
- [22] D. Fernandes, F. Costa, and E. Santos, "Digital-scalar PWM approaches applied to four-leg voltage-source inverters," *IEEE Trans. Ind. Electron.*, vol. 60, no. 5, pp. 2022–2030, May 2013.
- [23] J. A. Ali, M. A. Hannan, and A. Mohamed, "A novel quantum-behaved lightning search algorithm approach to improve the fuzzy logic speed controller for an induction motor drive," *Energies*, vol. 8, no. 11, pp. 13112–13136, Nov. 2015.
- [24] S. V. Ustun and M. Demirtas, "Modeling and control of V/f controlled induction motor using genetic-ANFIS algorithm," *Energy Conv. Manage.*, vol. 50, no. 3, pp. 786–791, Mar. 2009.
- [25] S. Sharma, P. Srivastava, X. Fang, and L. Kalin, "Performance comparison of adoptive neuro fuzzy inference system (ANFIS) with loading simulation program C++ (LSPC) model for streamflow simulation in El Niño Southern Oscillation (ENSO)-affected watershed," *Expert Syst. Appl.*, vol. 42, no. 4, pp. 2213–2223, Mar. 2015.
- [26] S. Adusumilli, D. Bhatt, H. Wang, P. Bhattacharya, and V. Devabhaktuni, "A low-cost INS/GPS integration methodology based on random forest regression," *Expert Syst. Appl.*, vol. 40, no. 11, pp. 4653–4659, Sep. 2013.
- [27] M. Liu, X. Liu, D. Liu, C. Ding, and J. Jiang, "Multivariable integration method for estimating sea surface salinity in coastal waters from in situ data and remotely sensed data using random forest algorithm," *Comput. Geosci.*, vol. 75, pp. 44–56, Feb. 2015.
- [28] H. Igelström, M. Emtner, E. Lindberg, and P. Åsenlöf, "Level of agreement between methods for measuring moderate to vigorous physical activity and sedentary time in people with obstructive sleep apnea and obesity," *Phys. Therapy*, vol. 93, pp. 50–59, Jan. 2013.
- [29] K. J. Stralen, K. J. Jager, C. Zoccali, and F. W. Dekker, "Agreement between methods," *Kidney Int.*, vol. 74, no. 9, pp. 1116–1120, Nov. 2008.



M. A. Hannan (M'10) received the B.Sc. degree in electrical and electronic engineering from the Chittagong University of Engineering and Technology, Chittagong, Bangladesh, in 1990, and the M.Sc. and Ph.D. degrees in electrical, electronic, and systems engineering from the Universiti Kebangsaan Malaysia (UKM), Bangi, Malaysia, in 2003 and 2007, respectively.

He was a Professor in the Department of Electrical, Electronic and Systems Engineering, UKM. He is currently a Professor in the Department of Electrical Power Engineering, College of Engineering, Universiti Tenaga Nasional, Kajang, Malaysia. His research interests include intelligent controllers, power electronics, hybrid vehicles, energy storage systems, image and signal processing, and artificial intelligence.



Jamal Abd Ali received the B.Sc. degree in electrical and electronics engineering from the University of Technology, Baghdad, Iraq, in 2005, the M.Sc. degree in power engineering from the College of Electrical and Electronic Engineering Techniques, Baghdad, Iraq, in 2010, and the Ph.D. degree in electrical and electronic engineering from the Department of Electrical, Electronics and Systems Engineering, Universiti Kebangsaan Malaysia, Bangi, Malaysia, in 2016.

He is with the South Electrical Station, General Company of Electricity Production Middle Region, Ministry of Electricity, Baghdad, Iraq. His research interests include intelligent controllers for induction motors using optimization methods to enhance performance efficiency.



Azah Mohamed (M'88–SM'05) received the B.Sc. degree from the University of London, London, U.K., in 1978, and the M.Sc. and Ph.D. degrees from the Universiti Malaya, Kuala Lumpur, Malaysia, in 1988 and 1995, respectively, all in electrical and electronic engineering.

She is currently a Professor in the Department of Electrical, Electronic and Systems Engineering, Universiti Kebangsaan Malaysia, Bangi, Malaysia. Her main research interests include power system security, power quality, and

artificial intelligence.



Mohammad Nasir Uddin (S'99–M'00–SM'04) received the B.Sc. and M.Sc. degrees in electrical and electronic engineering from the Bangladesh University of Engineering and Technology, Dhaka, Bangladesh, in 1993 and 1996, respectively, and the Ph.D. degree in electrical engineering from the Memorial University of Newfoundland, St. John's, NF, Canada, in 2000.

He is currently a Professor with the Department of Electrical Engineering, Lakehead University, Thunder Bay, ON, Canada, where he is engaged in teaching and research. His research interests include power electronics, electric motor drives, and applications of neural networks.